Published in final edited form as:
Neuroimage. 2012 February 15; 59(4): 3967–3975. doi:10.1016/j.neuroimage.2011.10.076.

The contribution of myelin to magnetic susceptibility-weighted contrasts in high-field MRI of the brain

Jongho Lee[1,2], **Karin Shmueli**[1], **Byeong-Teck Kang**[3,4], **Bing Yao**[1], **Masaki Fukunaga**[5], **Peter van Gelderen**[1], **Sara Palumbo**[6], **Francesca Bosetti**[6], **Afonso C. Silva**[3], and **Jeff H. Duyn**[1]

[1]Advanced MRI Section, Laboratory of Functional and Molecular Imaging, National Institute of Neurological Disorders and Stroke, National Institutes of Health, Bethesda, Maryland, USA

[2]Department of Radiology, University of Pennsylvania, Philadelphia, Pennsylvania, USA

[3]Cerebral Microcirculation Unit, Laboratory of Functional and Molecular Imaging, National Institute of Neurological Disorders and Stroke, National Institutes of Health, Bethesda, Maryland, USA

[4]Department of Veterinary Internal Medicine, College of Veterinary Medicine, Chungbuk National University, Cheongju, Chungbuk, Korea

[5]Biofunctional Imaging, WPI Immunology Frontier Research Center, Osaka University, Osaka, Japan

[6]Brain Physiology and Metabolism Section, National Institute of Aging, National Institutes of Health, Bethesda, Maryland, USA

Abstract

T_2*-weighted gradient-echo MRI images at high field (≥ 7 Tesla) have shown rich image contrast within and between brain regions. The source for these contrast variations has been primarily attributed to tissue magnetic susceptibility differences. In this study, the contribution of myelin to both T_2* and frequency contrasts is investigated using a mouse model of demyelination based on a cuprizone diet. The demyelinated brains showed significantly increased T_2* in white matter and a substantial reduction in gray-white matter frequency contrast, suggesting that myelin is a primary source for these contrasts. Comparison of *in-vivo* and *in-vitro* data showed that, although tissue T_2* values were reduced by formalin fixation, gray-white matter frequency contrast was relatively unaffected and fixation had a negligible effect on cuprizone-induced changes in T_2^* and frequency contrasts.

Keywords

T_2^* decay; R_2^* relaxation; phase image; resonance frequency image; demyelination; cuprizone; formalin fixation

Address correspondence to: Jongho Lee, 3 W Gates Building, 3400 Spruce St, Philadelphia, PA 19104, TEL: (215) 349-8462, FAX: (215) 349-5579, jonghoyi@upenn.edu.

Introduction

In recent years, T_2*-weighted gradient-echo MRI has revealed rich contrast between and within tissue types in both normal and diseased brains (Li et al., 2006; Duyn et al., 2007; Hammond et al., 2008; Marques et al., 2009; Budde et al., 2010). At high field (7 T and above), contrast in T_2*-weighted MRI is dominated by magnetic susceptibility effects, which can affect both the magnitude and the phase (through resonance frequency changes) of the MRI signal. Multiple sources and mechanisms underlying contrast in T_2*-weighted MRI have been suggested and identified, including iron (Ogg et al., 1999; Haacke et al., 2005; Yao et al., 2009; Fukunaga et al., 2010; Schweser et al., 2011), myelin (Ogg et al., 1999; Li et al., 2009; Liu et al., 2011; Zhong et al., 2011), deoxyhemoglobin (Reichenbach et al., 1997; Haacke et al., 2004; Sedlacik et al., 2008; Marques et al., 2009; Lee et al., 2010a; Petridou et al., 2010), calcium (Wu et al., 2009; Schweser et al., 2010), macroscopic geometry (Chu et al., 1990; Schäfer et al., 2009a; Shmueli et al., 2009), microstructural orientation (Wiggins et al., 2008; He and Yablonskiy, 2009; Schäfer et al., 2009b; Bender and Klose, 2010; Lee et al., 2010b; Liu, 2010; Denk et al., 2011; Lee et al., 2011) and chemical exchange (Zhong et al., 2008; Luo et al., 2010; Shmueli et al., 2011).

The relative contribution of the sources underlying magnetic susceptibility-weighted contrast has been found to vary across brain regions, and in certain regions, a single source may dominate. For example, tissue iron has been found to dominate T_2* contrast in the basal ganglia and various intracortical regions (Ogg et al., 1999; Haacke et al., 2005; Yao et al., 2009; Fukunaga et al., 2010; Hopp et al., 2010; Fukunaga et al., 2011), and deoxyhemoglobin is responsible for venous contrast (Reichenbach et al., 1997; Haacke et al., 2004). Interestingly, the role of myelin is less well established despite its well-recognized biological importance. One reason for this is that, unlike iron, the magnetic susceptibility of myelin is not known and is difficult to measure.

There are several pieces of evidence supporting a significant role of myelin in T_2* relaxation in the brain. One is the observation of diamagnetic frequency contrast in white matter relative to gray matter detected after iron extraction, suggesting that iron-free myelinated white matter is more diamagnetic than iron-free gray matter (Fukunaga et al., 2010). This notion of a negative frequency shift induced by a diamagnetic myelin susceptibility is further affirmed by recent findings in mouse models of demyelination (Baxan et al., 2010; Liu et al., 2011), and a study of human neonates (Zhong et al., 2011) which both showed reduced gray-white matter frequency contrast when myelin is mostly absent. In addition, several studies have found a dependence of T_2* on white matter fiber orientation relative to B_0, consistent with the notion that diamagnetic and anisotropically structured myelin would result in microscopic field variations that are orientation dependent (Wiggins et al., 2008; Schäfer et al., 2009b; Bender and Klose, 2010; Denk et al., 2011; Lee et al., 2011; Wiggins et al., 2011). Importantly, this orientation dependence was found to be rather strong, modulating R_2* (=1/T_2*) by about 60% in *in-vivo* brain at 7 T (Sati et al., 2011; Wiggins et al., 2011). Finally, variation in myelin density rather than iron content explained T_2* variation observed in a recent study of selected white matter fiber bundles (Li et al., 2009).

Despite these findings, which support an important role for myelin in magnetic susceptibility-weighted contrast, a direct link between tissue myelin content and T_2* relaxation has not been established. To address this, we used a mouse model of cuprizone-induced demyelination (Blakemore, 1973) to investigate the contribution of myelin to T_2* both *in vivo* and in formalin fixed tissue *in vitro*.

Materials and Methods

Cuprizone diet

Cuprizone (bis-cyclohexanone oxalyldihydrazone) is a copper chelator and is known to induce demyelination in the central nervous system when it is ingested as a mixture of food (Blakemore, 1973). A cuprizone mouse model has previously been used to demonstrate changes in several MRI properties such as T_1, T_2, diffusion, magnetization transfer and phase contrasts (Zhang et al.; Merkler et al., 2005; Song et al., 2005; Sun et al., 2006; Wu et al., 2008; Zaaraoui et al., 2008; Baxan et al., 2010).

MRI scans

All procedures were performed under a NIH-approved animal protocol, in accordance with NIH guidelines. Fourteen 8-week-old male C57BL/6 mice were used for this study. Cuprizone (Sigma, St. Louise, MO) was mixed into the powdered diet (0.2% of the diet weight) prepared by Research Diet Inc (New Brunswick, NJ), as previously described (Palumbo et al., 2011a; Palumbo et al., 2011b). Mice were fed *ad libitum* with either the cuprizone (n = 8) or a control diet (n = 6) for 6 weeks, and then underwent MRI scans. Just prior to MRI, the cuprizone-treated group had an average weight of 16.1 ± 2.3 g compared to 28.3 ± 4.3 g for the control group.

A 7 T animal MRI scanner (30 cm bore diameter, Bruker BioSpin, Ettlingen, Germany) was used to measure T_2* and frequency contrast. The system has a 15-cm gradient system (Resonance Research, Billerica, MA) which delivers up to 450 mT/m gradients in 130 μs. A custom-designed 1.27 cm diameter surface coil was used for signal reception and a body coil was used for signal transmission.

For *in-vivo* scans, animals were initially anesthetized with 5% isoflurane and then switched to 2% isoflurane during MRI scans. Animals were secured in a stereotaxic head-holder using a tooth bar and ear bars. The rectal temperature was monitored and maintained at 37 ºC using a circulating warm water channel. The MRI scan was started with a localizer, followed by transmitter and receiver gain calibrations and region-of-interest-based shimming (MAPSHIM, Bruker). After that, high resolution 2D multi-echo gradient-echo (GRE) data were acquired for magnitude and phase images, which were used to calculate T_2* maps and frequency contrast respectively. Four coronal slices were scanned with in-plane resolution = 50 × 50 μm^2, slice thickness = 0.75 mm, slice gap = 0.25 mm, FOV = 5.12 × 5.12 cm^2, TR = 1.5 s, TE = 6/13/20 ms and flip angle = 70°. The total scan time was 25.6 min. The locations of the slices were approximately at Bregma +1, 0, −1, and −2 mm (Franklin and Paxinos, 2007).

After MRI, each mouse was intracardially perfused with saline followed by 10% formalin solution. The brains were extracted from the skull and stored in 10% formalin for fixation. After a week of fixation, each brain was placed in the center of a tube (diameter = 16 mm, and length = 120 mm) and the tube was filled with phosphate buffered saline (PBS). The brains were rescanned at room temperature with the same parameters as *in vivo*. The long axis of the tube was aligned along the B_0 field of the magnet.

Histological staining

For one cuprizone-fed mouse and one normal mouse, brains were stained for myelin. First, the brains were cryoprotected using 30% sucrose solution and then cut on a cryostat (LI-COR, Bioscience, Lincoln, NE). Histology was performed on 30-μm-thick coronal sections using a Gallyas stain (Pistorio et al., 2006) to demonstrate the difference in myelination between the two samples.

MRI data processing

First, the complex raw data were reconstructed using a two-dimensional fast Fourier transform. The absolute and phase values of the resulting complex image data were used to form magnitude and phase images respectively. The phase images were unwrapped using a 2D unwrapping method (Jenkinson, 2003) and low-spatial-frequency background field variations were removed using a 2D high-pass Gaussian filter (FWHM = 19 voxels) within a hand-drawn mask that excluded areas with large off-resonance frequency offsets. Frequency images were calculated by dividing each phase image by its echo time and by 2π and then averaging the frequency images over the three echo times. T_2* maps were estimated by fitting a straight line to the log of the measured magnitude values against echo time by least-squares error estimation.

After generating all the T_2* and frequency images, the images from different animals were aligned together to generate averaged images. First, *in-vivo* frequency images of all control and cuprizone-treated mice were aligned to frequency images of one of the cuprizone-treated mice using a 2D linear registration program (Smith et al., 2004). Then, all the realigned frequency images were averaged to generate a temporary averaged frequency image. The individual frequency images were realigned to this temporary averaged frequency image to refine the registration. The registration was further improved by manually aligning the frequency images in the superior-inferior direction. After that, these results were averaged to form final averaged frequency images. Three averaged images were generated: one ‘total’ average over all mice (both cuprizone-treated and controls), one cuprizone group average and a control group average. The total average was used for drawing regions of interest (ROIs) as described below and the cuprizone and control group average images were compared to investigate the effects of demyelination. Note that ROIs were drawn on the total averaged images of the cuprizone-treated and control mice because the gray-white matter boundary was not clear in certain slices of the cuprizone mice.

The alignment parameters from the frequency images were applied to the T_2* images and total, cuprizone, and control group average images were created. The same alignment and averaging process was applied to the *in-vitro* dataset. To quantify cuprizone-induced frequency contrast changes, ROIs were manually drawn in gray matter (cortex) and white matter (corpus callosum) on the total averaged frequency images (*in vivo* and *in vitro* separately). The same ROIs were also used for T_2* quantification. Student’s t-tests were performed on each pair of conditions (i.e. cuprizone vs. control, *in-vivo* vs. *in-vitro*, and gray vs. white matter). Statistical significance was assessed using a threshold of $p = 0.05$. Since each comparison was performed on each pair of conditions individually, there was no need to adjust the significance threshold for multiple comparisons.

Because the average body weight between the two groups was different (16.1 ± 2.3 g for cuprizone and 28.3 ± 4.3 g for control), we tested whether the body weight had any influence on the measured contrasts. Within each group, the individual animal’s body weight was regressed out from the frequency, T_2* gray, T_2* white, and T_2* gray-white contrasts measured *in vivo* and *in vitro* (a total of 8 measured contrasts in each group). Then a p-value was calculated for each contrast. To account for multiple comparisons, we used a Bonferroni correction and considered only differences with $p < 0.05/8 = 0.0063$ to be significant. The brain image area was also measured to check the difference in brain size between the two groups. The first echo image from the *in-vivo* data was used to draw an ROI following the boundary of brain and the brain area was calculated as the number of voxels in this ROI.

Results

Among the 14 mice, one cuprizone-treated mouse showed enlarged ventricles and was excluded from further processing to avoid misalignment. As a result, 7 cuprizone-treated mice and 6 control mice were aligned to generate the results shown here.

The MRI results from *in-vivo* mouse brains are shown in Fig. 1. The total average frequency images over all mice and the ROIs for gray matter (cortex) and white matter (corpus callosum) are shown in Fig. 1A. When the control group average frequency images (Fig. 1B) are compared to the cuprizone group average frequency images (Fig. 1C), a significant reduction in gray-white matter contrast is observed in the cuprizone-treated mice. The measured gray-white matter frequency contrast was 3.58 ± 0.91 Hz (all values will be presented as mean ± standard deviation throughout this paper) and 1.45 ± 0.43 Hz in the control and cuprizone-treated mice respectively. This difference was statistically significant ($p = 6.5 \times 10^{-4}$). Images acquired *in vivo* suffered severely from artifacts that were most likely to originate from poor shims, physical motion, and B_0 fluctuation (Noll and Schneider, 1994) as these artifacts are not present in the fixed tissues (Fig. 2). It should be noted that, because the background field variation was removed from the frequency images during processing, only the relative contrast (e.g. between gray and white matter) is meaningful in the frequency images. This is unlike T_2^* for which absolute values are meaningful.

The T_2* measurement also showed reduced gray-white matter T_2* contrast in the cuprizone-treated mice (Figs. 2D and E). In the control group, the mean gray matter T_2* was 34.0 ± 3.3 ms (R_2* = 29.6 ± 3.0 Hz) whereas the mean T_2* in white matter was 28.4 ± 3.4 ms (R_2* = 35.7 ± 4.6 Hz) yielding a moderately significant gray-white matter difference (p = 0.007). In comparison, the cuprizone-treated group had a gray matter T_2* of 37.2 ± 1.2 ms (R_2* = 26.9 ± 0.9 Hz) and a white matter T_2* of 39.4 ± 2.8 ms (R_2* = 25.5 ± 1.7 Hz) and these gray-white matter values were not significantly different (p = 0.055). The mean T_2* in gray matter showed a marginally significant increase in the cuprizone group relative to the controls (p = 0.033). The mean white matter T_2* values were significantly increased in the cuprizone-treated mice compared to controls ($p = 5.3 \times 10^{-5}$). These ROI results and statistical tests are summarized in Fig. 3 and Table 1.

These *in-vivo* results were corroborated by the measurements *in vitro* which showed superior image quality and reduced ROI standard deviations (Fig. 2). The gray-white matter frequency contrast was 3.91 ± 0.43 Hz in the control group and 1.10 ± 0.31 Hz in the cuprizone group which was significantly different ($p = 1.4 \times 10^{-7}$) (Figs. 2B and C). The mean T_2* values in control mice (Figs. 2D) were significantly different (p = 0.0013) in gray matter 30.3 ± 2.4 ms (R_2* = 33.2 ± 2.9 Hz) compared to white matter 25.2 ± 1.8 ms (R_2* = 39.8 ± 3.1 Hz). However, there was no significant difference between the mean gray (T_2* = 33.3 ± 2.2 ms; R_2* = 30.1 ± 2.1 Hz) and white (T_2* = 32.6 ± 2.2 ms; R_2* = 30.8 ± 2.1 Hz) matter T_2* values in the cuprizone-fed group (p = 0.29). Comparing mean T_2* values between the cuprizone-fed and control groups, there was a significant increase ($p = 1.9 \times 10^{-5}$) in the white matter T_2* in the cuprizone-treated mice relative to the controls. The mean gray matter T_2* values were marginally increased in the cuprizone-treated mice relative to the controls (p = 0.02) suggesting that the cuprizone diet also affected gray matter in addition to the strong effects found in white matter.

Tissue fixation effects

To test the effects of tissue fixation on frequency contrast and T_2* values, the results obtained in fixed tissues were compared to the measurements made *in vivo*. The gray-white matter frequency contrast was not significantly changed by fixation (p = 0.22 for the control

group and p = 0.066 for the cuprizone group) suggesting that formalin fixation had little effect on frequency contrast. On the other hand, the T_2* values were reduced in the fixed tissues compared to the values *in vivo*: in the control group, the gray matter T_2* was reduced by 3.7 ± 1.7 ms (p = 0.025) and the white matter by 3.1 ± 1.6 ms (p = 0.044). In the cuprizone group, the gray matter T_2* decreased by 3.9 ± 0.96 ms (p = 0.0014), and the white matter T_2* decreased by 6.8 ± 1.3 ms ($p = 1.53 \times 10^{-4}$). Despite overall decreases in T_2* values, the relative contrasts were sustained after fixation, giving a clear gray-white matter differentiation in control mice.

Previous studies have shown that formalin-fixation reduces T_1 and T_2 relaxation parameters (Kamman et al., 1985; Tovi and Ericsson, 1992; Yong Hing et al., 2005; Thelwall et al., 2006; Dawe et al., 2009; Shepherd et al., 2009a; Shepherd et al., 2009b). Hence, the reduced T_2* observed in fixed tissues may have been caused by a decrease in T_2 on fixation. Note that the reduced T_2* values observed in fixed brains may not have originated solely from the formalin fixation process as there was a temperature difference between the scans (i.e. 37 °C *in vivo* vs. room temperature *in vitro*).

Body weight and brain size

When the body weight of individual animals was regressed out from each contrast in each group, none of the contrasts showed a significant correlation with body weight for $p < 0.05/8 = 0.0063$ with Bonferroni correction for multiple comparisons. The p-values for the correlation of body weight with (i) gray-white matter frequency contrast were 0.33, 0.68, 0.39, and 0.11 for *in-vivo* control, *in-vivo* cuprizone, fixed control and fixed cuprizone groups respectively (the same order hereafter); (ii) gray matter T_2* values: 0.14, 0.66, 0.54, and 0.11; (iii) white matter T_2* values: 0.22, 0.10, 0.40, and 0.015; and (iv) gray-white matter T_2* contrast: 0.95, 0.19, 0.95, 0.54. These results suggest that the body weight is not a major contributor to the contrast changes observed in the cuprizone-treated mice.

The brain size measured in the four slices was not significantly different between the two groups. The total number of voxels in the cuprizone-treated group was 70236 ± 887 voxels whereas it was 69122 ± 1610 voxels in the control group and the resulting p-value was 0.09.

Myelin staining

The myelin stained images, approximately at Bregma = 1.3 mm, (Franklin and Paxinos, 2007), show a similar pattern of changes to those observed in T_2* and frequency contrast images (Fig. 4). Demyelination of the corpus callosum was evident in the cuprizone-treated mouse.

These results suggest that myelination is a major source of T_2* and frequency contrast between gray and white matter in these mouse brains.

Discussion

In this study, we have investigated the effect of demyelination on MRI T_2* and frequency (phase) contrasts using a cuprizone mouse model. The results show a significant decrease in frequency contrast between gray and white matter, a substantial increase of T_2* in white matter and a marginal increase of T_2* in gray matter in cuprizone-treated animals relative to controls. These changes suggest that myelin is an important source of T_2* and frequency contrast in brain parenchyma. Our results using the cuprizone mouse model of demyelination are in agreement with previous frequency contrast studies of dysmyelination in a shiverer mouse model (Liu et al., 2011) and of low or absent myelination in human neonates (Zhong et al., 2011).

In this study, we also investigated the effects of tissue fixation on T_2* and frequency contrasts, and found that frequency contrast between gray and white matter is minimally affected by fixation. On the other hand, T_2* values in these tissues were significantly reduced by fixation. We attribute these divergent effects of fixation to changes in the microscopic tissue structure, which may preferentially affect T_2* through changes in microscopic (or sub-voxel) field gradients. Alternatively, changes in water diffusion or tissue water content could also differentially affect T_2* and frequency contrasts.

In our analysis, the brains were realigned and averaged to draw ROIs. This was necessary because the cuprizone-treated group did not show a clear gray-white matter tissue boundary. Despite our efforts to realign the brains as closely as possible, realignment errors due to individual variability and small differences in slice positioning were unavoidable and some structures (e.g. internal capsule) were not well visualized in the averaged images due to partial volume effects.

Demyelination in cuprizone-fed mice

The secondary effects of the cuprizone treatment are a primary limitation of the current study. Cuprizone is known to specifically affect mature oligodendrocytes, which then fail to fulfill their high metabolic demand and undergo apoptosis (Matsushima and Morell, 2001; Palumbo et al., 2011b). Cuprizone also causes an inflammatory response in the brain but without disrupting the blood-brain barrier (McMahon et al., 2002). To our knowledge, specific effects of cuprizone on brain perfusion or hemoglobin saturation have not been investigated and remain an uncertainty in this study. In addition, it is plausible that the cuprizone diet may have affected other tissue constituents, such as proteins, which may affect T_2* and frequency contrast. Such confounds from other sources are also present in previous studies (Liu et al., 2011; Zhong et al., 2011). For example, shiverer mice are deficient in myelin basic protein (Popko et al., 1987) and neonatal brains have a different concentration of iron than adult brains (Hallgren and Sourander, 1958). Despite the confounding factors being different in each study, the common factor in all these studies is that the myelination changes. The results of these studies agree in the sense that reduced myelination decreases the gray-white matter contrast. Hence, myelin is likely to be an important source of gray-white matter T_2* and frequency contrasts. Compared to shiverer mice, whose myelin concentration is low throughout their life span, the cuprizone treatment used in this study induces temporary demyelination in adult animals. If cuprizone is later removed from the diet, remyelination occurs spontaneously.

Cuprizone may also remove certain types of iron from the white matter, most importantly the iron storage protein ferritin. However, the concentration of iron in the corpus callosum is low (White et al., 1999; Sergeant et al., 2005). Furthermore, a decreased iron concentration is expected to lead to a more negative frequency shift which is inconsistent with the observed increase in the white matter frequency relative to gray matter in the cuprizone group compared to the controls (Figs 1B,C and 2B,C). At the same time, it is unlikely that cuprizone predominantly affected the gray matter as the strongest T_2* increases between the control and cuprizone groups were observed in the white matter.

Unlike previous studies (Liu et al., 2011; Zhong et al., 2011), the current study includes the effects of demyelination on T_2* values and the effects of fixation on T_2* and frequency contrasts. Because frequency images contain only relative contrast information, one cannot argue with certainty that the reduced gray-white matter frequency contrast in the cuprizone-treated mice results from a susceptibility change in white matter. Rather, the reduced frequency contrast between gray and white matter could also have been caused by a change in gray matter susceptibility. The fact that the predominant T_2* change was observed in the white matter suggests that the reduction in frequency contrast was probably caused by

changes in the susceptibility of white matter. In other words, the results suggest a white matter frequency increase rather than a gray matter frequency decrease. This example illustrates the importance of investigating both T_2* and frequency changes.

Compared to the 1.95 Hz frequency contrast between gray and white matter measured at 9.4 T in control mice (Liu et al., 2011), our results at 7 T show a larger gray-white matter frequency contrast (3.91 Hz). This discrepancy may originate from differences in the age and type of animals used. In addition, different ROIs were used and the high-pass filtering included here in the processing significantly affects the frequency contrast (Chen et al., 2010).

In the current study, small increases in gray matter T_2* were observed in cuprizone-treated mice. This may be related to cuprizone-induced reductions of the myelin in gray matter (Norkute et al., 2009).

In the cuprizone-treated mouse images, different white matter structures show different contrast changes. For example, the anterior commissures in Figs. 1, 2 and 4 (labeled in Fig. 2) show stronger gray-white matter contrast than the corpus callosum. It has been reported that cuprizone treatment causes different levels of demyelination in different white matter regions (Stidworthy et al., 2003; Yang et al., 2009). The heterogeneity in the maturation of white matter has been suggested as a possible reason for the differential effects of cuprizone treatment (Yang et al., 2009). In our study, we focused on the corpus callosum because it is one of the structures most strongly affected by cuprizone treatment.

It is interesting to consider that, from the data presented here, one may be able to derive a rough estimate of the magnetic susceptibility of myelin. Let us assume that the water protons that contribute to the measured MRI signal are predominantly found in elongated compartments (e.g. cylinders) outside the myelin itself (He and Yablonskiy, 2009), and that their susceptibility-mediated transverse relaxation (characterized by T_2' or R_2') is dominated by static dephasing effects. In that case, the shifts in resonance frequency and R_2' (Δf and $\Delta R_2'$ respectively) attributed to the susceptibility of myelin are related and can be approximated by (Yablonskiy and Haacke, 1994; He and Yablonskiy, 2009):

$$\Delta f = \gamma \cdot 0.5 \cdot \Delta\chi \cdot B_0 \cdot \sin^2\theta \cdot s \quad [1]$$

$$|\Delta R_2'| = 2\pi \cdot \gamma \cdot 0.5 \cdot |\Delta\chi| \cdot B_0 \cdot \sin^2\theta \cdot s \quad [2]$$

where γ is the gyromagnetic ratio in $Hz \cdot T^{-1}$; $\Delta\chi$ is the magnetic susceptibility difference between myelin and the surrounding medium; B_0 is main magnetic field strength ($\gamma \cdot B_0$ = 298 MHz at 7T); θ is the angle between the B_0 field and the cylinders; and s is the volume fraction of myelin. Note that these equations were derived based on SI units ($\chi_{SI} = 4\pi\chi_{CGS}$), and that large-scale (supra-voxel) susceptibility effects were ignored. In our experiments, Δf and $|\Delta R_2'|$ were −2.13 Hz and 10.2 Hz respectively, where Δf was approximated by the white-gray matter frequency contrast difference between the control and cuprizone groups *in vivo* (neglecting potential bulk frequency shifts from the sparser and more randomly

oriented myelin in gray matter) and $\Delta R_2'$ was approximated by the R_2^* difference in white matter between the two groups *in vivo*. Further, if we consider that the white matter fibers of the mouse corpus callosum run predominantly perpendicular to the B_0 field (i.e. $\theta = 90°$), and assume the volume fraction of myelin in white matter to be 16% (O'Brien and Sampson, 1965), $\Delta\chi$ calculated from the Δf and $|\Delta R_2'|$ values given above using Eq. 1 and Eq. 2 is found to be −0.089 and −0.068 ppm respectively. The sign used for $\Delta\chi$ calculated from $|\Delta R_2'|$ was taken from the sign of $\Delta\chi$ calculated from Δf because $|\Delta R_2'|$ is independent of sign. The relatively low myelin susceptibility estimated from $|\Delta R_2'|$ may be related to our assumption that the protons are primarily in the static dephasing regime which may not be fully valid. These $\Delta\chi$ values are in good agreement with the reported susceptibility of mouse corpus callosum (−0.0132 ppm) (Liu et al., 2011) when taking into account the 16% myelin volume fraction.

Tissue iron, copper, and chemical exchange

Other sources of T_2^* and frequency contrast include tissue iron, copper, and chemical exchange. It has been shown that tissue iron is an important source of T_2^* and frequency contrasts (Ogg et al., 1999; Haacke et al., 2005; Yao et al., 2009; Fukunaga et al., 2010). In mice, the concentrations of iron in cortex and corpus callosum are similar and substantially lower than those in human brains (White et al., 1999; Sergeant et al., 2005). Therefore, tissue iron may not contribute to gray-white matter contrasts in the mouse as much as it does in humans, although this needs further investigation.

Because cuprizone is a copper chelator, it is reasonable to suggest that copper could be another source for the observed changes. Little is known about the effects of copper on T_2^* and frequency contrast. The concentration of copper is ~2.6 – 4 times lower than iron in the C57B6/D2 mouse (Sergeant et al., 2005) and its susceptibility is close to that of water (slightly more diamagnetic) (Schenck, 1996). Therefore, it may not have significant effects.

Chemical exchange of protons between free water and macromolecules is another source of gray-white matter frequency contrast (Zhong et al., 2008; Luo et al., 2010; Shmueli et al., 2011). It has been shown that white matter has a positive exchange-induced frequency shift compared to gray matter and this is opposite to the overall gray-white matter frequency contrast observed *in vivo* (Shmueli et al., 2011). This suggests that the chemical-exchange-induced gray-white matter frequency difference acts together with and in opposition to an even greater susceptibility-induced gray-white matter frequency contrast. In the current study, demyelination in the cuprizone-fed mice is likely to reduce macromolecules in white matter as suggested in a magnetization transfer study (Zaaraoui et al., 2008). This reduction in macromolecules is expected to lead to a corresponding reduction in chemical-exchange-induced frequency shifts in the white matter. Such a reduction would increase the overall gray-white matter frequency difference because the exchange-induced frequency shifts generally oppose the susceptibility-induced frequency shifts (Luo et al., 2010; Shmueli et al., 2011). The decreased gray-white matter frequency contrast observed in the cuprizone-treated mice suggests that the effect of cuprizone on the exchange-induced component of the frequency contrast was smaller than on the susceptibility-induced component.

Tissue fixation effects

The effects of tissue fixation on MRI parameters have been an important topic of research as a large number of studies have been performed in fixed tissues and the results were used to infer the contrast expected *in vivo*. Most studies have focused on T_1, T_2 and diffusion changes, revealing decreased T_1, T_2 and water diffusivity after fixation (Kamman et al., 1985; Tovi and Ericsson, 1992; Yong Hing et al., 2005; Thelwall et al., 2006; Dawe et al., 2009; Shepherd et al., 2009a; Shepherd et al., 2009b). It has also been shown that the

decreased relaxation parameters and diffusivity can be restored once tissues are soaked in PBS (Shepherd et al., 2009b). To our knowledge, however, no previous study has demonstrated T_2* and frequency contrast changes after fixation. Note that the temperature also differed between the scans: from 37°C *in vivo* to room temperature for the fixed tissues. Therefore, this temperature difference could also have contributed to the observed contrast changes. Since most fixed tissue studies are performed at room temperature, it is useful to demonstrate the combined effects of fixation and temperature rather than separating out the effect of fixation.

Recently, a dependence of T_2* on fiber orientation has been observed in brain white matter and it has been suggested to use this dependence to map fiber orientation and to study white matter integrity (Lee et al., 2011). The measured change in T_2* for fibers parallel vs. perpendicular to B_0 (ΔT_2*) was only 3 ms in fixed tissue (Lee et al., 2011) but reached up to 15 ms *in vivo* (Wiggins et al., 2011) suggesting that fixation has a large effect on ΔT_2*. The current study suggests that this decrease in ΔT_2* on fixation could be partly due to an overall reduction in T_2 and T_2* values on fixation.

Conclusion

Myelin is a considerable source of magnetic susceptibility-weighted contrast between gray and white matter at high field (7 T). Both T_2* and frequency contrast are substantially reduced in mice with significant myelin loss induced by a cuprizone diet. This finding holds true for experiments both *in vivo* and *in vitro*, and has implications for the interpretation of T_2* and frequency contrast across brain regions. The sign of the observed frequency changes with demyelination are consistent with a diamagnetic susceptibility of myelin; this conforms a previously suggested notion that iron and myelin differentially affect T_2* and frequency contrast originating from tissue magnetic susceptibility.

Acknowledgments

This research was supported (in part) by the Intramural Research Program of the NIH, NINDS.

The authors appreciate useful comments from Dr. Hang Joon Jo at NIH.

References

Baxan, N.; Harsan, L-A.; Dragonu, I.; Merkle, A.; Hennig, J.; von Elverfeldt, D. Myelin as a primary source of phase contrast demonstrated in vivo in the mouse brain. Proceedings of the 18th Annual Meeting of ISMRM; Stockholm, Sweden. 2010. p. 3016

Bender B, Klose U. The in vivo influence of white matter fiber orientation towards B0 on T2* in the human brain. NMR Biomed. 2010; 23:1071–1076. [PubMed: 20665897]

Blakemore W. Demyelination of the superior cerebellar peduncle in the mouse induced by cuprizone. J Neurol Sci. 1973; 20:63–72. [PubMed: 4744511]

Budde J, Shajan G, Hoffmann J, Uurbil K, Pohmann R. Human imaging at 9.4 T using T2*, phase, and susceptibility weighted contrast. Magn Reson Med. 2010 available online.

Chen Z, Johnston LA, Kwon DH, Oh SH, Cho ZH, Egan GF. An optimised framework for reconstructing and processing MR phase images. Neuroimage. 2010; 49:1289–1300. [PubMed: 19818859]

Chu SC, Xu Y, Balschi JA, Springer CS Jr. Bulk magnetic susceptibility shifts in NMR studies of compartmentalized samples: use of paramagnetic reagents. Magn Reson Med. 1990; 13:239–262. [PubMed: 2156125]

Dawe RJ, Bennett DA, Schneider JA, Vasireddi SK, Arfanakis K. Postmortem MRI of human brain hemispheres: T2 relaxation times during formaldehyde fixation. Magn Reson Med. 2009; 61:810–818. [PubMed: 19189294]

Denk C, Torres EH, MacKay A, Rauscher A. The influence of white matter fibre orientation on MR signal phase and decay. NMR Biomed. 2011; 24:246–252. [PubMed: 21404336]

Duyn JH, van Gelderen P, Li TQ, de Zwart JA, Koretsky AP, Fukunaga M. High-field MRI of brain cortical substructure based on signal phase. Proc Natl Acad Sci USA. 2007; 104:11796–11801. [PubMed: 17586684]

Franklin, KBJ.; Paxinos, G. The mouse brain in stereotaxic coordinates. 3. Academic press; 2007.

Fukunaga M, Li TQ, van Gelderen P, de Zwart JA, Shmueli K, Yao B, Lee J, Maric D, Aronova MA, Zhang G. Layer-specific variation of iron content in cerebral cortex as a source of MRI contrast. Proc Natl Acad Sci U S A. 2010; 107:3834–3839. [PubMed: 20133720]

Fukunaga, M.; van Gelderen, P.; Lee, J.; Li, T-Q.; de Zwart, JA.; Merkle, H.; Matsuda, KM.; Matsuura, E.; Duyn, JH. Investigation of magnetic susceptibility contrast across cortical grey matter and white matter. Proceedings of the 19th Annual Meeting of ISMRM; Montreal, Canada. 2011. p. 12

Haacke EM, Cheng NYC, House MJ, Liu Q, Neelavalli J, Ogg RJ, Khan A, Ayaz M, Kirsch W, Obenaus A. Imaging iron stores in the brain using magnetic resonance imaging. Magn Reson Imaging. 2005; 23:1–25. [PubMed: 15733784]

Haacke EM, Xu Y, Cheng YC, Reichenbach JR. Susceptibility weighted imaging (SWI). Magn Reson Med. 2004; 52:612–618. [PubMed: 15334582]

Hallgren B, Sourander P. The effect of age on the non-haemin iron in the human brain. Journal of Neurochemistry. 1958; 3:41–51. [PubMed: 13611557]

Hammond KE, Lupo JM, Xu D, Metcalf M, Kelley DAC, Pelletier D, Chang SM, Mukherjee P, Vigneron DB, Nelson SJ. Development of a robust method for generating 7.0 T multichannel phase images of the brain with application to normal volunteers and patients with neurological diseases. Neuroimage. 2008; 39:1682–1692. [PubMed: 18096412]

He X, Yablonskiy DA. Biophysical mechanisms of phase contrast in gradient echo MRI. Proc Natl Acad Sci USA. 2009; 106:13558–13563. [PubMed: 19628691]

Hopp K, Popescu BFG, McCrea RPE, Harder SL, Robinson CA, Haacke ME, Rajput AH, Rajput A, Nichol H. Brain iron detected by SWI high pass filtered phase calibrated with synchrotron X ray fluorescence. J Magn Reson Imaging. 2010; 31:1346–1354. [PubMed: 20512886]

Jenkinson M. Fast, automated, N-dimensional phase-unwrapping algorithm. Magn Reson Med. 2003; 49:193–197. [PubMed: 12509838]

Kamman R, Go K, Stomp G, Hulstaert C, Berendsen H. Changes of relaxation times T1 and T2 in rat tissues after biopsy and fixation. Magn Reson Imaging. 1985; 3:245–250. [PubMed: 3908869]

Lee J, Hirano Y, Fukunaga M, Silva AC, Duyn JH. On the contribution of deoxy-hemoglobin to MRI gray-white matter phase contrast at high field. Neuroimage. 2010a; 49:193–198. [PubMed: 19619663]

Lee J, Shmueli K, Fukunaga M, van Gelderen P, Merkle H, Silva AC, Duyn JH. Sensitivity of MRI resonance frequency to the orientation of brain tissue microstructure. Proc Natl Acad Sci U S A. 2010b; 107:5130–5135. [PubMed: 20202922]

Lee J, van Gelderen P, Kuo L, Merkle H, Silva AC, Duyn JH. T2*-based fiber orientation mapping. Neuroimage. 2011; 57:225–234. [PubMed: 21549203]

Li T, Yao B, van Gelderen P, Merkle H, Dodd S, Talagala L, Koretsky A, Duyn J. Characterization of T2* heterogeneity in human brain white matter. Magn Reson Med. 2009; 62:1652–1657. [PubMed: 19859939]

Li TQ, van Gelderen P, Merkle H, Talagala L, Koretsky AP, Duyn J. Extensive heterogeneity in white matter intensity in high-resolution T2*-weighted MRI of the human brain at 7.0 T. Neuroimage. 2006; 32:1032–1040. [PubMed: 16854600]

Liu C. Susceptibility tensor imaging. Magn Reson Med. 2010; 63:1471–1477. [PubMed: 20512849]

Liu C, Li W, Johnson GA, Wu B. High-field (9.4 T) MRI of brain dysmyelination by quantitative mapping of magnetic susceptibility. Neuroimage. 2011; 56:930–938. [PubMed: 21320606]

Luo J, He X, d'Avignon DA, Ackerman JJH, Yablonskiy DA. Protein-induced water 1H MR frequency shifts: Contributions from magnetic susceptibility and exchange effects. J Magn Reson. 2010; 202:102–108. [PubMed: 19879785]

Marques JP, Maddage R, Mlynarik V, Gruetter R. On the origin of the MR image phase contrast: An in vivo MR microscopy study of the rat brain at 14.1 T. Neuroimage. 2009; 46:345–352. [PubMed: 19254768]

Matsushima GK, Morell P. The neurotoxicant, cuprizone, as a model to study demyelination and remyelination in the central nervous system. Brain Pathology. 2001; 11:107–116. [PubMed: 11145196]

McMahon EJ, Suzuki K, Matsushima GK. Peripheral macrophage recruitment in cuprizone-induced CNS demyelination despite an intact blood-brain barrier. J Neuroimmunology. 2002; 130:32–45. [PubMed: 12225886]

Merkler D, Boretius S, Stadelmann C, Ernsting T, Michaelis T, Frahm J, Brück W. Multicontrast MRI of remyelination in the central nervous system. NMR Biomed. 2005; 18:395–403. [PubMed: 16086436]

Noll, DC.; Schneider, W. Respiration artifacts in functional brain imaging: sources of signal variation and compensation strategies. Proceedings of the Society of Magnetic Resonance; San Francisco, USA. 1994. p. 647

Norkute A, Hieble A, Braun A, Johann S, Clarner T, Baumgartner W, Beyer C, Kipp M. Cuprizone treatment induces demyelination and astrocytosis in the mouse hippocampus. J Neurosci Res. 2009; 87:1343–1355. [PubMed: 19021291]

O'Brien JS, Sampson EL. Lipid composition of the normal human brain: gray matter, white matter, and myelin. J Lipid Res. 1965; 6:537–544. [PubMed: 5865382]

Ogg RJ, Langston JW, Haacke EM, Steen RG, Taylor JS. The correlation between phase shifts in gradient-echo MR images and regional brain iron concentration. Magn Reson Imaging. 1999; 17:1141–1148. [PubMed: 10499676]

Palumbo, S.; Toscano, C.; Parente, L.; Weigert, R.; Bosetti, F. Prostaglandins, Leukotrienes and Essential Fatty Acids. 2011a. Time-dependent changes in the brain arachidonic acid cascade during cuprizone-induced demyelination and remyelination.

Palumbo S, Toscano CD, Parente L, Weigert R, Bosetti F. The cyclooxygenase 2 pathway via the PGE2 EP2 receptor contributes to oligodendrocytes apoptosis in cuprizone induced demyelination. J Neurochem. 2011b

Petridou N, Wharton SJ, Lotfipour A, Gowland P, Bowtell R. Investigating the effect of blood susceptibility on phase contrast in the human brain. Neuroimage. 2010; 50:491–498. [PubMed: 20026280]

Pistorio AL, Hendry SH, Wang X. A modified technique for high-resolution staining of myelin. J Neurosci Methods. 2006; 153:135–146. [PubMed: 16310256]

Popko B, Puckett C, Lai E, Shine HD, Readhead C, Takahashi N. Myelin deficient mice: expression of myelin basic protein and generation of mice with varying levels of myelin. Cell. 1987; 48:713–721. [PubMed: 2434243]

Reichenbach JR, Venkatesan R, Schillinger DJ, Kido DK, Haacke EM. Small vessels in the human brain: MR venography with deoxyhemoglobin as an intrinsic contrast agent. Radiology. 1997; 204:272–277. [PubMed: 9205259]

Sati P, Silva AC, van Gelderen P, Gaitan MI, Wohler JE, Jacobson S, Duyn JH, Reich DS. In vivo quantification of T2* anisotropy in white matter fibers in marmoset monkeys. Neuroimage. 2011 (available online).

Schäfer A, Wharton S, Gowland P, Bowtell R. Using magnetic field simulation to study susceptibility-related phase contrast in gradient echo MRI. Neuroimage. 2009a; 48:126–137.

Schäfer, A.; Wiggins, CJ.; Turner, R. Understanding the orientation dependent T2* contrast of the cingulum in ultra high fields. Proceedings of the 17th Annual Meeting of ISMRM; Honolulu, Hawaii. 2009b. p. 955

Schenck JF. The role of magnetic susceptibility in magnetic resonance imaging: MRI magnetic compatibility of the first and second kinds. Med Phys. 1996; 23:815–850. [PubMed: 8798169]

Schweser F, Deistung A, Lehr B, Reichenbach J. Quantitative imaging of intrinsic magnetic tissue properties using MRI signal phase: an approach to in vivo brain iron metabolism? Neuroimage. 2011; 54:2789–2807. [PubMed: 21040794]

Schweser F, Deistung A, Lehr BW, Reichenbach JR. Differentiation between diamagnetic and paramagnetic cerebral lesions based on magnetic susceptibility mapping. Medical physics. 2010; 37:5165–5178. [PubMed: 21089750]

Sedlacik J, Kutschbach C, Rauscher A, Deistung A, Reichenbach JR. Investigation of the influence of carbon dioxide concentrations on cerebral physiology by susceptibility-weighted magnetic resonance imaging (SWI). Neuroimage. 2008; 43:36–43. [PubMed: 18678260]

Sergeant C, Vesvres M, Devès G, Guillou F. Calcium, potassium, iron, copper and zinc concentrations in the white and gray matter of the cerebellum and corpus callosum in brain of four genetic mouse strains. Nucl Instr Meth Phys Res B. 2005; 231:234–238.

Shepherd TM, Flint JJ, Thelwall PE, Stanisz GJ, Mareci TH, Yachnis AT, Blackband SJ. Postmortem interval alters the water relaxation and diffusion properties of rat nervous tissue--Implications for MRI studies of human autopsy samples. Neuroimage. 2009a; 44:820–826. [PubMed: 18996206]

Shepherd TM, Thelwall PE, Stanisz GJ, Blackband SJ. Aldehyde fixative solutions alter the water relaxation and diffusion properties of nervous tissue. Magn Reson Med. 2009b; 62:26–34. [PubMed: 19353660]

Shmueli K, de Zwart JA, van Gelderen P, Li TQ, Dodd SJ, Duyn JH. Magnetic susceptibility mapping of brain tissue in vivo using MRI phase data. Magn Reson Med. 2009; 62:1510–1522. [PubMed: 19859937]

Shmueli K, Dodd SJ, Li TQ, Duyn JH. The contribution of chemical exchange to MRI frequency shifts in brain tissue. Magn Reson Med. 2011; 65:35–43. [PubMed: 20928888]

Smith SM, Jenkinson M, Woolrich MW, Beckmann CF, Behrens TE, Johansen-Berg H, Bannister PR, De Luca M, Drobnjak I, Flitney DE. Advances in functional and structural MR image analysis and implementation as FSL. Neuroimage. 2004; 23:S208–219. [PubMed: 15501092]

Song SK, Yoshino J, Le TQ, Lin SJ, Sun SW, Cross AH, Armstrong RC. Demyelination increases radial diffusivity in corpus callosum of mouse brain. Neuroimage. 2005; 26:132–140. [PubMed: 15862213]

Stidworthy MF, Genoud S, Suter U, Mantei N, Franklin RJM. Quantifying the Early Stages of Remyelination Following Cuprizone induced Demyelination. Brain Pathology. 2003; 13:329–339. [PubMed: 12946022]

Sun SW, Liang HF, Trinkaus K, Cross AH, Armstrong RC, Song SK. Noninvasive detection of cuprizone induced axonal damage and demyelination in the mouse corpus callosum. Magn Reson Med. 2006; 55:302–308. [PubMed: 16408263]

Thelwall PE, Shepherd TM, Stanisz GJ, Blackband SJ. Effects of temperature and aldehyde fixation on tissue water diffusion properties, studied in an erythrocyte ghost tissue model. Magn Reson Med. 2006; 56:282–289. [PubMed: 16841346]

Tovi M, Ericsson A. Measurements of T1 and T2 over time in formalin-fixed human whole-brain specimens. Acta Radiologica. 1992; 33:400–404. [PubMed: 1389643]

White AR, Reyes R, Mercer JFB, Camakaris J, Zheng H, Bush AI, Multhaup G, Beyreuther K, Masters CL, Cappai R. Copper levels are increased in the cerebral cortex and liver of APP and APLP2 knockout mice. Brain research. 1999; 842:439–444. [PubMed: 10526140]

Wiggins, CJ.; Gudmundsdottir, V.; Le Bihan, D.; Lebon, V.; Chaumeil, M. Orientation dependence of white matter T2* contrast at 7 T: A direct demonstration. Proceedings of the 16th Annual Meeting of ISMRM; Toronto, Canada. 2008. p. 237

Wiggins, G.; Wiggins, C.; Zhang, B.; Brown, B.; Stoeckel, B.; Sodickson, D. Exploring orientation dependence of T2* in white matter by extreme rotation of the human head at 7 tesla. Proceedings of the 19th Annual Meeting of ISMRM; Montreal, Canada. 2011. p. 13

Wu QZ, Yang Q, Cate HS, Kemper D, Binder M, Wang HX, Fang K, Quick MJ, Marriott M, Kilpatrick TJ. MRI identification of the rostral caudal pattern of pathology within the corpus callosum in the cuprizone mouse model. J Magn Reson Imaging. 2008; 27:446–453. [PubMed: 17968901]

Wu Z, Mittal S, Kish K, Yu Y, Hu J, Haacke EM. Identification of calcification with MRI using susceptibility weighted imaging: A case study. J Magn Reson Imaging. 2009; 29:177–182. [PubMed: 19097156]

Yablonskiy DA, Haacke EM. Theory of NMR signal behavior in magnetically inhomogeneous tissues: the static dephasing regime. Magn Reson Med. 1994; 32:749–763. [PubMed: 7869897]

Yang HJ, Wang H, Zhang Y, Xiao L, Clough RW, Browning R, Li XM, Xu H. Region-specific susceptibilities to cuprizone-induced lesions in the mouse forebrain: Implications for the pathophysiology of schizophrenia. Brain research. 2009; 1270:121–130. [PubMed: 19306847]

Yao B, Li TQ, Gelderen PV, Shmueli K, de Zwart JA, Duyn JH. Susceptibility contrast in high field MRI of human brain as a function of tissue iron content. Neuroimage. 2009; 44:1259–1266. [PubMed: 19027861]

Yong Hing CJ, Obenaus A, Stryker R, Tong K, Sarty GE. Magnetic resonance imaging and mathematical modeling of progressive formalin fixation of the human brain. Magn Reson Med. 2005; 54:324–332. [PubMed: 16032673]

Zaaraoui W, Deloire M, Merle M, Girard C, Raffard G, Biran M, Inglese M, Petry KG, Gonen O, Brochet B. Monitoring demyelination and remyelination by magnetization transfer imaging in the mouse brain at 9.4 T. MAGMA. 2008; 21:357–362. [PubMed: 18779984]

Zhang J, Jones MV, McMahon MT, Mori S, Calabresi PA. In vivo and ex vivo diffusion tensor imaging of cuprizone induced demyelination in the mouse corpus callosum. Magn Reson Med. Available online.

Zhong K, Ernst T, Buchthal S, Speck O, Anderson L, Chang L. Phase contrast imaging in neonates. Neuroimage. 2011; 55:1068–1072. [PubMed: 21232619]

Zhong K, Leupold J, von Elverfeldt D, Speck O. The molecular basis for gray and white matter contrast in phase imaging. Neuroimage. 2008; 40:1561–1566. [PubMed: 18353683]

Highlights

1. Cuprizone-induced demyelination increased WM T_2* and reduced GM-WM T_2* contrast.
2. GM-WM frequency (phase) contrast was also reduced.
3. Tissue fixation decreased T_2* values but did not affect GM-WM frequency contrast.

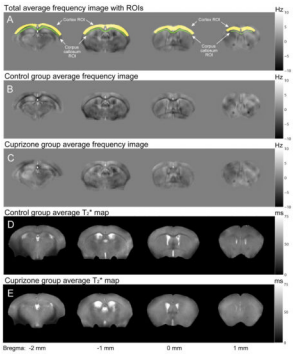

Figure 1.

Averaged frequency images and T_2* maps in control and cuprizone-treated mice *in vivo*. Compared to the control (B and D), the cuprizone-treated mice (C and E) show significantly reduced gray-white matter contrasts both in frequency and T_2*. ROIs are colored in yellow for the cortex (gray matter) and green for the corpus callosum (white matter).

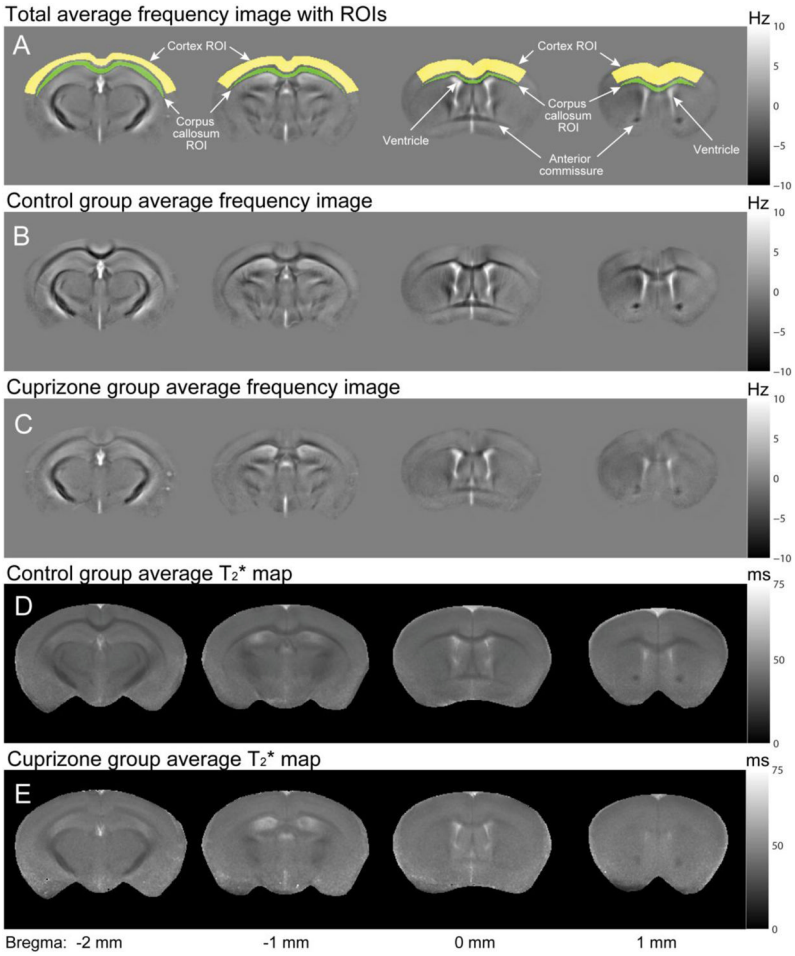

Figure 2.

Average frequency images and T_2* maps in control and cuprizone-treated fixed mouse brains *in vitro*. *In-vitro* images also show reduced frequency and T_2* contrasts in cuprizone-treated mice relative to controls, as observed *in vivo*. Image quality is superior to *in-vivo* images, most likely due to improved shimming and reduced motion-related artifacts.

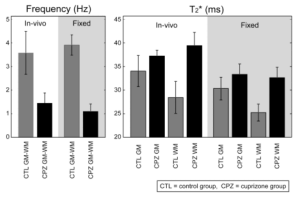

Figure 3.

Frequency and T_2* results with t-test comparisons: the cuprizone diet significantly reduced the gray-white matter frequency and T_2* contrasts. Fixation only induced significant changes in T_2* values.

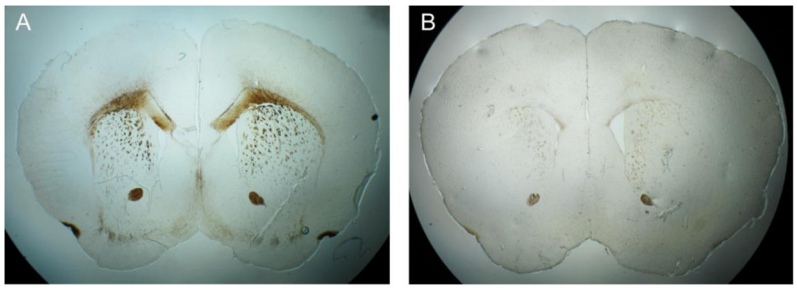

Figure 4.

Myelin stained images from (A) a control mouse brain and (B) a cuprizone-treated mouse brain. The cuprizone-treated mouse brain shows significantly reduced staining in the corpus callosum. The slices were approximately at Bregma + 1.3 mm (Franklin and Paxinos, 2007)

Table 1

Statistical comparisons are given together with the p-values obtained from t-tests. Significant differences ($p < 0.05$) are highlighted with a *.

	Comparison		p-value	Significance $p < 0.05$
Frequency contrast	In-vivo CTL GM-WM	In-vivo CPZ GM-WM	6.5×10^{-4}	*
	Fixed CTL GM-WM	Fixed CPZ GM-WM	1.4×10^{-7}	*
	In-vivo CTL GM-WM	Fixed CTL GM-WM	0.22	
	In-vivo CPZ GM-WM	Fixed CPZ GM-WM	0.066	
T_2* contrast	In-vivo CTL GM	In-vivo CTL WM	0.007	*
	In-vivo CPZ GM	In-vivo CPZ WM	0.055	
	In-vivo CTL GM	In-vivo CPZ GM	0.033	*
	In-vivo CTL WM	In-vivo CPZ WM	5.3×10^{-5}	*
	Fixed CTL GM	Fixed CTL WM	0.0013	*
	Fixed CPZ GM	Fixed CPZ WM	0.29	
	Fixed CTL GM	Fixed CPZ GM	0.02	*
	Fixed CTL WM	Fixed CPZ WM	1.9×10^{-5}	*
	In-vivo CTL GM	Fixed CTL GM	0.025	*
	In-vivo CTL WM	Fixed CTL WM	0.044	*
	In-vivo CPZ GM	Fixed CPZ GM	0.0014	*
	In-vivo CPZ WM	Fixed CPZ WM	1.53×10^{-4}	*

CTL = control group and CPZ = cuprizone treated group